Reliability-based Design Optimization of Offshore Wind Turbine Concrete Structures

Joey Velarde
Ph.D. Student, Dept. of Marine & Foundation Engineering, COWI A/S, Aarhus, Denmark

Claus Kramhøft
Chief Specialist, Dept. of Marine & Foundation Engineering, COWI A/S, Aarhus, Denmark

John Dalsgaard Sørensen
Professor, Dept. of Civil Engineering, Aalborg University, Aalborg, Denmark

ABSTRACT: Structural design optimization of offshore wind turbine support structures can significantly contribute to energy cost reductions. In this paper, an application of reliability-based design optimization is presented for a concrete gravity-based foundation, where an optimal combination of steel reinforcements and prestressing steel is desired. Extreme load distribution is derived based on environmental contour method for a reference offshore site. Illustrative results show that an optimal design can be found that satisfies the required structural reliability levels for all limit states considered with the least amount of material.

1. INTRODUCTION

Within the last few years, offshore wind energy has become a mature technology due to the continuous reduction of levelized cost of energy (LCOE). In addition to the increase in wind turbine capacity, the design optimization of both wind turbine components and offshore foundations has significantly contributed in making offshore wind energy a cost-competitive renewable energy source.

Offshore wind turbine (OWT) support structures have to be designed for combined extreme wind and wave loads. Although there is no clear consensus on metocean data extrapolation within the academic and industrial community, a recommended standard approach in the design code (IEC, 2009) is to use the traditional inverse first order reliability method (IFORM) introduced by Winterstein et al. (1993).

In this study, IFORM is applied to derive the environmental contours for a reference offshore site at the central North Sea. Using an integrated OWT model, time-domain simulations are performed to derive the extreme load distribution and to evaluate fatigue damage at a critical section of an offshore foundation. An example of reliability-based design optimization (RBDO) is presented for a concrete gravity based foundation (GBF), where an optimal combination of steel reinforcements and prestressing steel is desired, assuming that the overall geometry of the concrete structure is already known. The structural reliability is evaluated against four simplified limit states, which includes yielding of steel reinforcement (ULS), compressive failure of concrete (ULS), and concrete fatigue (FLS) both on the compressive and tensile cases.

2. ENVIRONMENTAL CONTOUR METHOD

2.1. Description of Metocean Data

The derivation of extreme sea states is based on 5 years of metocean data (Platform 62304), which were collected and made freely available by the *MyOcean project* and the programs that contribute to it. Hourly 10-minute mean wind speed measured from 15 m AMSL are converted to hub height (90 m AMSL) wind speeds, assuming a power law profile with power law coefficient, $\alpha = 0.15$. The wind rose at the selected location is shown in Figure 1. For ULS design purposes, wind speeds at the dominant direction (210-240 deg) are further considered.

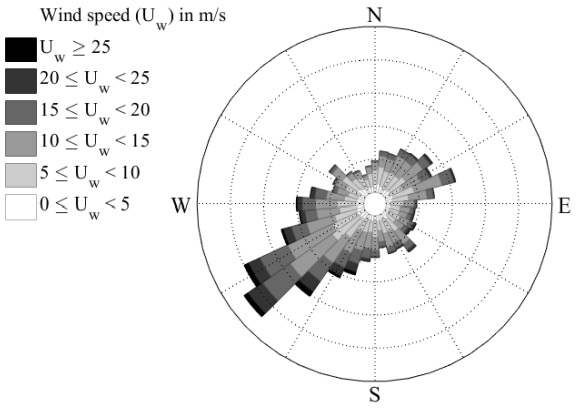

Figure 1: Site wind rose plot. Dominant direction (210-240 degrees) is considered for the analysis

2.2. Environmental Contour Method

The environmental contour (EC) method, introduced by Winterstein (1993), is a widely used approach for derivation of design loads, particularly for offshore structures. It allows decoupling of the uncertainties related to the dynamic structural response and environmental conditions, since the latter is represented by contours independent of the structure. As opposed to the forward first-order reliability method (FORM) (Madsen, Krenk, & Lind, 2006), where the failure probability (P_F) is sought for a given reliability problem, the inverse-FORM (IFORM) seeks for all possible design points for a given reliability level or probability of failure (P_F). For a given marginal distribution and conditional distribution, the standard normal random variables (u_1, u_2) can be mapped into the physical space (U_w, H_s) using Rosenblatt transformation (Rosenblatt, 1952):

$$\Phi(u_1) = F_{U_w}(v) \tag{1}$$

$$\Phi(u_2) = F_{H_s|U_w}(h \mid v) \tag{2}$$

For a given probability of exceedance (q), the equivalent radius (β_q) in standard Gaussian space can be calculated as follows:

$$\beta_q = \Phi^{-1}(1 - P_F) = \Phi^{-1}(1 - \frac{q}{\lambda_{1hr}}) \tag{3}$$

where λ_{1hr} is the expected annual number of 1-hour sea states above the chosen threshold, i.e. if all hourly observations is considered, then λ_{1hr} = 365x24 = 8760 observations per year. When applying peak-over-threshold (POT) approach, λ_{1hr} can be approximated by the number of observations above the threshold divided by the length of data in years.

2.2.1. Marginal U_w distribution

The marginal extreme U_w distribution is derived using POT data that satisfy two thresholds: (1) U_w above cut-out wind speed (U_w>25 m/s) and (2) U_w are at least 40 hours apart to satisfy independence assumption (Vanem, 2015). Figure 2 illustrates the extreme U_w marginal distribution estimated by a Gumbel distribution:

$$F_{U_w}(v) = \exp\left(-\exp\left(-\frac{v - \alpha_v}{\beta_v}\right)\right) \tag{4}$$

where α_v and β_v are the distribution parameters found by fitting the curve to the POT data.

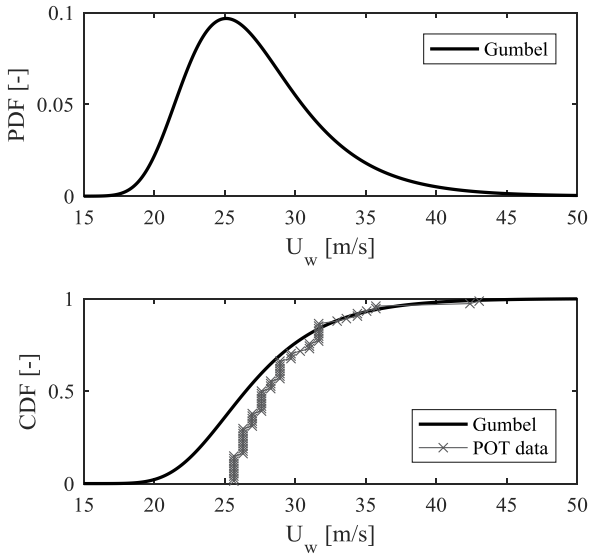

Figure 2: Extreme wind speed marginal distribution with Gumbel fit to upper 80% quantile (α_v = 25.1 m/s, β_v = 3.8 m/s). Wind speeds are at hub height.

2.2.2. Conditional H_s distribution

The distribution of H_s conditional to mean U_w is estimated by:

$$F_{H_s|U_w}(h \mid v) = \Phi\left(\frac{h-\mu_h}{\sigma_h}\right) \quad (5)$$

where μ_h and σ_h are the mean and standard deviation of the normal distribution, respectively. Figure 3 illustrates the estimation of μ_h and σ_h based on the binned POT data. Based on Equations 4 and 5, the site-dependent joint probability density for extreme U_w and H_s distribution is derived as shown in Figure 4

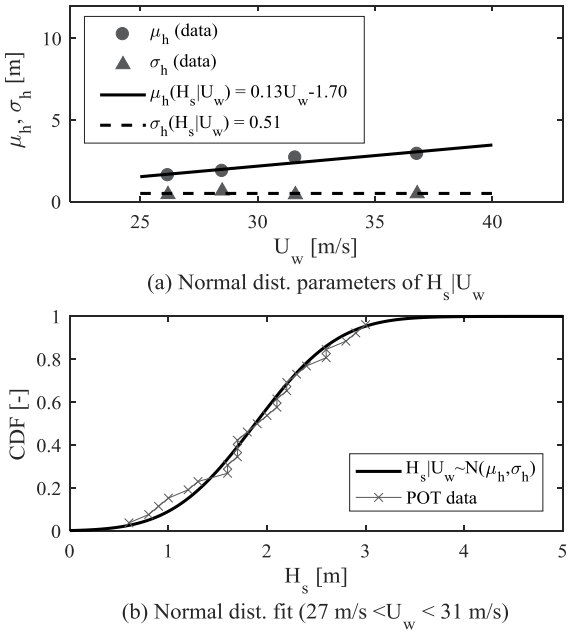

Figure 3: (a) Estimation of Normal distribution parameters for $H_s|U_w$; (b) $H_s|U_w$ data fit

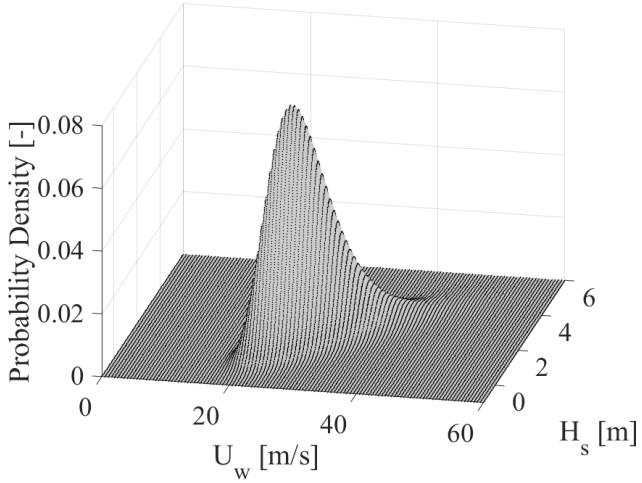

Figure 4: Joint probability density for extreme wind speed and wave height distribution

2.3. Design Sea States

The derived environmental contours for selected return periods (T_R) are compared to site data as shown in Figure 5. Depending on site characteristics and foundation section considered, the maximum response can be given by either sea states with the maximum U_w or with the maximum H_s. Both sets of design sea states are summarized in Table 1 and Table 2, respectively, and are used for derivation of design response in the succeeding section.

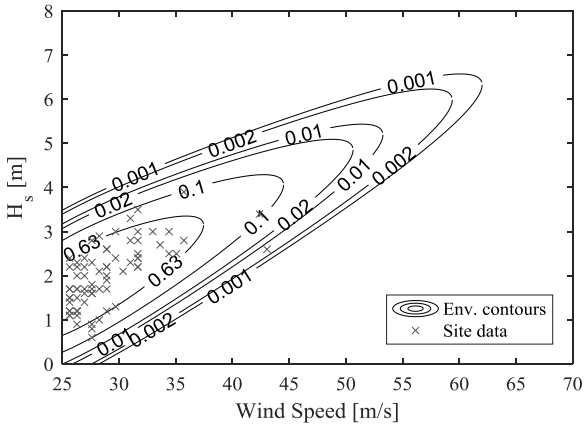

Figure 5: Derived environmental contours for selected annual probability of exceedance (q)

Table 1: Design sea states for maximum wind speed

q [-]	*T_R [yr]*	*U_w [m/s]*	*H_s [m]*	*T_p [s]*
0.63	*1*	*37.4*	*3.17*	*7.95*
0.10	*10*	*44.5*	*4.10*	*8.84*
0.02	*50*	*50.6*	*4.90*	*9.54*
0.01	*100*	*53.3*	*5.24*	*9.83*
0.002	*500*	*59.4*	*6.04*	*10.44*
0.001	*1000*	*62.0*	*6.38*	*10.68*

Table 2: Design sea states for maximum wave height

q [-]	*T_R [yr]*	*U_w [m/s]*	*H_s [m]*	*T_p [s]*
0.63	*1*	*35.9*	*3.35*	*8.13*
0.10	*10*	*42.7*	*4.29*	*9.02*
0.02	*50*	*48.8*	*5.09*	*9.71*
0.01	*100*	*51.6*	*5.44*	*9.98*
0.002	*500*	*57.7*	*6.23*	*10.58*
0.001	*1000*	*60.2*	*6.57*	*10.81*

The wave peak period (T_p) shown is the mean T_p given H_s, estimated using a linear H_s-T_p relation based on wind farm data.

3. CASE STUDY: THORNTON BANK

The reinforced concrete GBFs supporting the Thornton Bank offshore wind turbines (Phase 1) are selected to demonstrate the derivation of extreme response distribution. Figure 6 illustrates the OWT model installed at a mean water depth of 25 m AMSL.

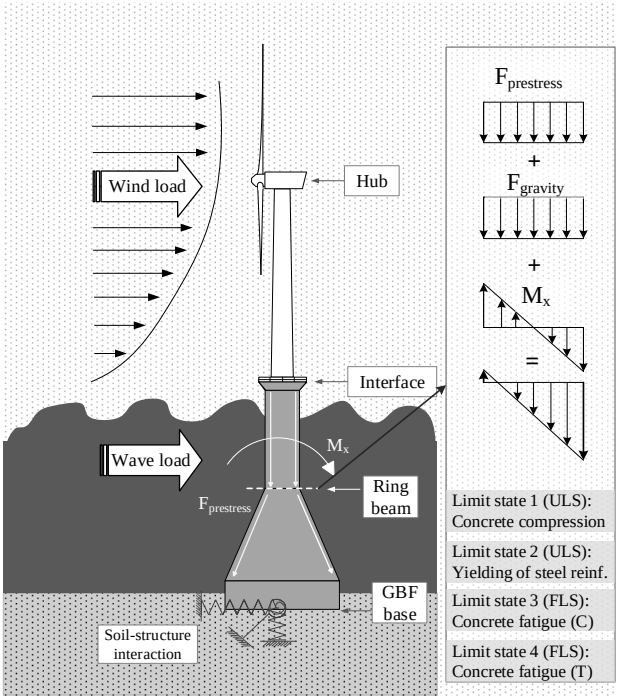

Figure 6: GBF model and limit states

3.1. Wind Turbine Integrated Model

An integrated structural model is developed in the simulation tool HAWC2 (Larsen & Hansen, 2015), which is based on a multibody formulation with Timoshenko beam elements. The NREL 5 MW reference wind turbine (Jonkman, Butterfield, Musial, & Scott, 2009) is used with the aerodynamic loads calculated from blade element momentum theory. Hydrodynamic loads are calculated using Morison's equation (Morison, Johnson, Schaaf, & others, 1950), where the wave coefficients are calibrated to account for diffraction effects and secondary steel. More details on the integrated model can be found in Velarde et al. (2018).

3.2. Extreme Load Distribution

Assuming that the extreme responses are given by either maximum mean wind speed U_w or maximum significant wave height H_s, the annual maximum load (M_x) at critical sections is approximated as the mean of 10 realizations. Based on a simplified design load case for parked wind turbines (DLC 6.1), the calculated M_x is shown in Figure 7. In this case, design sea states at maximum U_w result to 5-7% higher loads, and thus govern the extreme loads distribution summarized in Table 3.

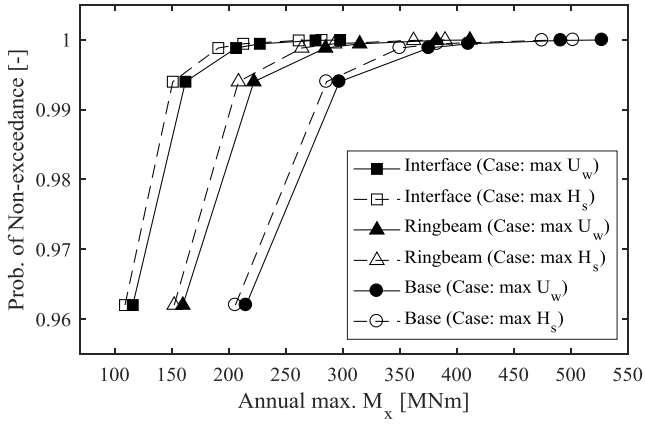

Figure 7: Annual maximum bending moment (M_x) distributions at different foundation sections

Table 3: Mean extreme bending moment (M_x) given by maximum U_w

q [-]	*T_R [yr]*	*M_x [MNm]*		
		Interface	*Ring beam*	*Base*
0.63	*1*	*115.9*	*159.8*	*215.2*
0.10	*10*	*162.1*	*222.0*	*297.1*
0.02	*50*	*206.5*	*284.9*	*375.4*
0.01	*100*	*227.3*	*314.8*	*410.2*
0.002	*500*	*276.1*	*382.1*	*491.2*
0.001	*1000*	*297.7*	*411.4*	*527.3*

Normally, variability in calculated response is accounted by inflating the environmental contours as demonstrated by Winterstein et al. (1993) for wave-dominated offshore structures. For offshore wind turbines, variability of response can be different and sensitivity to environmental input varies depending on the location of the substructure. For a more consistent approach in extreme response estimation, an 85% quantile is used in this study as recommended by Haver (2002). A Gumbel distribution demonstrates a

good fit to M_x as illustrated in Figure 8. The M_x distribution is defined by:

$$F_{M_x}(x) = \exp\left(-\exp\left(-\frac{x-\alpha_x}{\beta_x}\right)\right) \quad (6)$$

where α_x and β_x are the Gumbel distribution parameters found by fitting the curve to the POT data. The M_x distribution is used as a main input in ULS limit state functions.

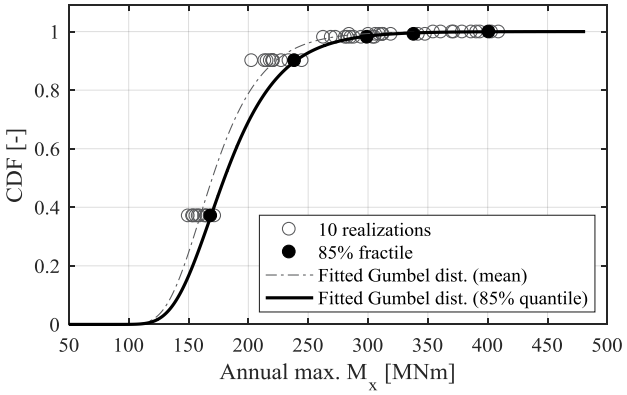

Figure 8: Gumbel distribution fit (α_x=168.5 MNm, β_x=31.5 MNm, mean value E[M_x]= 186.7 MNm and standard deviation σ_x=40.4 MNm) for 85% load quantile at ring beam

4. RELIABILITY ASSESSMENT

The structural reliability is assessed for four different limit states: concrete compressive failure (LS1), yielding of steel reinforcement (LS2), concrete fatigue failure under compressive loads (LS3), and concrete fatigue failure under tensile loads (LS4). Evaluation of reliability for different combinations of the decision parameters A_{ps} (area of prestressing steel) and A_s (area of reinforcements) provides a safe region, where the most optimal structural configuration can be achieved. The formulation of the four limit state functions (see Figure 6) are discussed in this section. The stochastic and deterministic parameters are summarized in Table 4.

4.1. Limit State 1: Concrete Compressive Failure

The first limit state considers concrete compressive failure under extreme loading conditions. The compressive strength varies depending on the concrete grade selected. For offshore foundations subjected to harsh environments, moderate to high grade concrete classes are normally used. In practice, direct samples and compressive tests are performed to verify the uncertainty in the compressive strength. Assuming a concrete grade (see Table 4) with mean compressive strength, f_c = 53.3 MPa, and characteristic compressive cylinder strength, f_{ck} = 44 MPa. A simplified model for the section bending moment (M_{cap}) capacity can be formulated as a function of A_s:

$$M_{cap} = A_s f_y X_{rs}\left(d_{As} - \frac{1}{2}\frac{A_s f_y X_{rs}}{d_o f_c X_c}\right) \quad (7)$$

where:

f_y steel yield strength [MPa]
A_s area of steel reinforcement [mm²]
d_{As} distance of reinf. from top of beam [mm]
d_o section outer diameter [mm]
X_{rs} steel resistance model uncertainty [-]
X_c concrete resistance model uncertainty [-]

Table 4: Stochastic and deterministic variables for limit states 1, 2, 3 and 4. N: Normal, LN: Lognormal, G: Gumbel, D: Deterministic

Type	*Var.*	*Dist.*	*Unit*	*Mean*	*Std. dev.*
Action	M_x	*G*	*MNm*	*186.7*	*40.4*
	W_G	*N*	*MN*	*22.0*	*0.5*
Material	f_c	*LN*	*MPa*	*53.3*	*5.33*
	f_{py}	*N*	*MPa*	*1643*	*41*
	f_y	*N*	*MPa*	*560*	*30*
Model Unc.	X_S	*LN*	-	*1.00*	*0.10*
	X_{ps}	*LN*	-	*1.00*	*0.05*
	X_{rs}	*LN*	-	*1.00*	*0.05*
	X_N	*LN*	-	*1.00*	*0.05*
	X_c	*LN*	-	*1.00*	*0.10*
	X_m	*N*	-	*1.50*	*0.75*
	Δ	*LN*	-	*1.00*	*0.40*
Structural	A_c	*D*	mm^2	*9.42E6*	-
	c	*D*	*mm*	*3.25E3*	-
	I	*D*	mm^4	*4.27E13*	-
	d_o	*D*	*mm*	*6.50E3*	-
	d_s	*D*	*mm*	3.00E3	-
	d_{As}	*D*	*mm*	6.25E3	-

The compressive strength (R_1) of the critical section is evaluated using the moment of inertia for a cracked section (I_{CR}). To simplify calculations for a hollow cylindrical section, I_{CR} is calculated by assuming that the neutral axis is not shifted. A reduction factor (A_s/A_{s0}) is calibrated to account for the change in concrete section contribution (I_o) to the total moment of inertia. The increase in I_{CR} due to additional reinforcements (A_s) at a given distance (d_s) from the neutral axis is accounted by transforming A_s to an equivalent concrete area (A_c) using the modular ratio, $n_{sc}=E_s/E_c$.

$$R_1 = \frac{M_{cap} c}{I_{CR}} \tag{8}$$

$$I_{CR} = \frac{I_o}{2}\left(\frac{A_s}{A_{s0}}\right) + n_{sc} A_s d_s^{\,2} \tag{9}$$

The load (S_1) is governed by the extreme annual bending moment (M_x) derived in the preceding section based on the procedure by Haver (2002; 2006). Additional compressive stress from prestressing steel (A_{ps}) and gravity loads (W_G) are considered. In practice, prestressing force is normally set to 80% of the characteristic yield strength (f_{py}'). To avoid unreasonable high stress contributions at higher quantiles of prestress strength, the prestress load is limited to a constant value of $0.80f_{py}$' such that the resulting load can be written:

$$S_1 = \frac{M_x c}{I_{CR}} X_S X_N + \frac{0.80 f_{py}' A_{ps}}{A_c} X_{ps} + \frac{W_G}{A_c} \tag{10}$$

where:

c radial distance to critical point [mm]
f_{py} prestressing steel yield strength [MPa]
A_c concrete area [mm^2]
X_{ps} prestressing uncertainty [-]
X_S load model uncertainty [-]
X_N load statistical uncertainty [-]

The limit state function for ultimate compressive failure is then written:

$$g_1(x) = R_1 - S_1 \tag{11}$$

4.2. Limit State 2: Yielding of Steel Rebars

Yielding of steel reinforcements before concrete compressive failure, also known as ductile failure, can occur at high flexural loads. The resistance to steel yielding (R_2) can be expressed as:

$$R_2 = f_y X_{rs} \tag{12}$$

Yielding occurs after tensile cracks have fully propagated, thus the tensile stress for steel is also calculated with a cracked section. The load at the steel rebars (S_2) is converted from concrete stress by the modular ratio (n_{sc}):

$$S_2 = n_{sc}\left(\frac{M_x d_s}{I_{CR}} X_S X_N - \left(\frac{f_{py} A_{ps}}{A_c} X_{ps} + \frac{W_G}{A_c}\right)\right) \tag{13}$$

The limit state function for ultimate compressive failure is given by:

$$g_2(x) = R_2 - S_2 \tag{14}$$

4.3. Limit State 3: Concrete Fatigue (C)

The third limit state evaluates fatigue reliability of concrete, considering the stresses are within the compression range. Based on wind farm data, 11 representative sea states with wind speeds within operating conditions is used for fatigue analysis in HAWC2. The time-dependent stresses on the compression side of the uncracked concrete section is estimated as a function of the axial load F_Y, prestressing force F_{PT}, bending moment M, and the transformed moment of inertia (I_{TR}):

$$\sigma_C(t) = \frac{F_Y(t) + F_{PT}(t)}{A_c} + \frac{M(t) c}{I_{TR}} \tag{15}$$

$$I_{TR} = I_o + (n_{sc} - 1) A_s d_s^{\,2} \tag{16}$$

Since concrete fatigue is also a function of the means stress level, the number of cycles to failure (N_i) is calculated from the maximum stress

(σ_{max}) and minimum stress (σ_{min}) for each stress cycle (i) and representative sea state (j). For each stress cycle determined from rainflow counting, fatigue damage is evaluated based on the DNV (2012) equation, which is modified by adding the stochastic variable X_m to account for the material uncertainty (Velarde et al., 2018):

$$\log_{10}(N_i) = \frac{C_1\left(1-S_{\max_{i,j}}\right)}{\left(1-S_{\min_{i,j}}\right)} + X_m \tag{17}$$

where:

$$S_{\max_{i,j}} = \left(\sigma_{mean_{i,j}} X_{LP} + \sigma_{amp_{i,j}} X_{LA}\right) \Big/ f_c \tag{18}$$

$$S_{\min_{i,j}} = \left(\sigma_{mean_{i,j}} X_{LP} - \sigma_{amp_{i,j}} X_{LA}\right) \Big/ f_c \tag{19}$$

The constant C_1 is taken equal to 10 for structures in water having stress variation within the compression range. It is assumed that wind turbine responses are not sensitive to the variation of A_s and A_{ps}. Rather, both A_s and A_{ps} affect the allowed number of cycles (N_i) through the I_{TR} and F_{PT}, respectively. The uncertainty terms X_{LP} and X_{LA} accounts for uncertainties in the mean and amplitude stresses, respectively. Using Equations 15 to 19, the fatigue damage (D_f) is calculated as:

$$D_f = \int_{U_{in}}^{U_{out}} \sum_{i,j} \frac{n_{i,j} T_L}{N_{i,j}\left(A_s, A_{ps}, X_{LP}, X_{LA}, X_m, f_c\right)} \tag{20}$$

Uncertainty analysis (Velarde et al., 2018) has shown that X_m governs the uncertainty in concrete fatigue, and that D_f can be approximated as:

$$D_f \approx D_{f0} \exp\left(-\lambda X_m\right) + \varepsilon_L \tag{21}$$

where D_{f0} is the base damage calculated using the design SN curve (X_m=0), with model parameter λ=2.3 and error term ε_L~N(0, 0.003) accounting for load uncertainty were calibrated from uncertainty analysis. Finally, the time-dependent fatigue limit state equation is formulated based on linear damage theory (Miner, 1945; Palmgren, 1924):

$$g_3(x,t) = \Delta - D_f(A_s, A_{ps}, X_m, t) \tag{22}$$

4.4. Limit State 4: Concrete Fatigue (T)

The fourth limit state also evaluates fatigue, and focuses on identifying the minimum amount of A_s and A_{ps} to limit tensile stresses at acceptable levels. The constant $C1$ is reduced to 8 (DNV, 2012) and the stresses on the tensile section evaluated as:

$$\sigma_T(t) = \frac{W_G(t) + F_{PT}(t)}{A_c} - \frac{M(t)c}{I_{TR}} \tag{23}$$

Following the same stochastic modeling as limit state 3, the limit state equation is written as:

$$g_4(x,t) = \Delta - D_f(A_s, A_{ps}, X_m, t) \tag{24}$$

5. RESULTS & DISCUSSION

The results of reliability assessment for the four limit states are illustrated in Figure 9, where the variations in the annual reliability index ($\Delta\beta$) is shown as a function of A_s & A_{ps}.

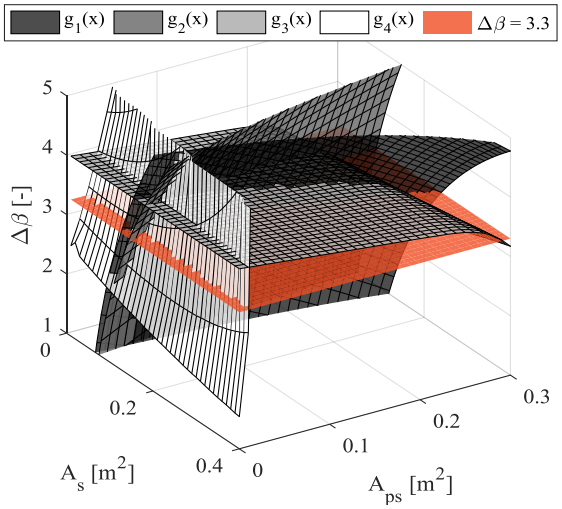

Figure 9: Graphical representation of annual reliability indices ($\Delta\beta_1$, $\Delta\beta_2$, $\Delta\beta_3$ & $\Delta\beta_4$)

Assuming an annual reliability index of $\Delta\beta$ = 3.3 for unmanned offshore structures (IEC, 2019), a graphical solution can be derived as shown in Figure 10. The "safe region" indicates combinations of A_s & A_{ps} that satisfy all the limit states considered. In this case study, it is shown that the choice of A_{ps} is governed by fatigue limit states $g_3(x)$ & $g_4(x)$, while the choice of A_s is governed by ULS compressive failure, $g_1(x)$.

Based on these results, an optimal design can be found which satisfies all the limit states considered with the least amount of material (A_s, A_{ps}).

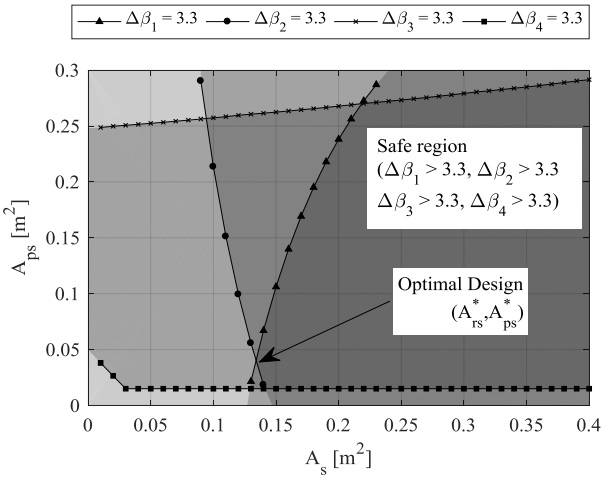

Figure 10: Graphical representation of optimal design (A_s, A_{ps}*)*

6. CONCLUSIONS

An application of RBDO for offshore wind turbine foundation is presented, where the design parameters (A_s, A_{ps}) are assessed against four simplified limit states. Ideally, a more accurate limit state formulations is desired, i.e. by use of nonlinear FE models as demonstrated by Kenna & Basu (2015). Due to this limitation, the optimal design is not directly comparable to the actual design. Nonetheless, the simplified assessment provides a good demonstration of RBDO.

Future work will focus on application of RBDO on defining primary geometry of support structures for offshore wind turbines.

7. ACKNOWLEDGEMENT

This research work was performed within the European project INFRASTAR, which has received funding from the European Union's Horizon 2020 research and innovation programme under the Marie Skłodowska-Curie grant agreement No 676139.

8. REFERENCES

DNV. (2012). Offshore Concrete Structures--DNV OS-C502. *Det Norsk Veritas, Norway*.

Haver, S. (2002). On the prediction of extreme wave crest heights. In *Seventh International Workshop on Wave Hindcasting and Forecasting, Banff, AB, Canada, Oct*.

Haver, S. (2006). Reasons for Focusing More on Prediction of the Very Extreme Sea States. In *9th International Workshop on Wave Hindcasting and Forecasting*.

IEC. (2019). IEC 61400-1: Wind energy generation systems - Part 1: Design requirements. *International Electrotechnical Commission*.

IEC. (2009). IEC 61400-3: Wind turbines--part 3: Design requirements for offshore wind turbines. *International Electrotechnical Commission, Geneva*.

Jonkman, J., Butterfield, S., Musial, W., & Scott, G. (2009). *Definition of a 5-MW reference wind turbine for offshore system development*.

Kenna, A., & Basu, B. (2015). A finite element model for pre-stressed or post-tensioned concrete wind turbine towers. *Wind Energy*, *18*(9), 1593–1610.

Larsen, T. J., & Hansen, A. M. (2015). *How 2 HAWC2, the user's manual*.

Madsen, H. O., Krenk, S., & Lind, N. C. (2006). *Methods of structural safety*. Courier Corporation.

Miner, M. A. (1945). Cumulative damage in fatigue. *American Society of Mechanical Engineers - Journal of Applied Mechanics*, *12*(3), 159–164.

Morison, J. R., Johnson, J. W., Schaaf, S. A., & others. (1950). The force exerted by surface waves on piles. *Journal of Petroleum Technology*, *2*(05), 149–154.

Palmgren, A. (1924). Die lebensdauer von kugellagern. *Zeitschrift Des Vereins Deutscher Ingenieure*, *68*(14), 339–341.

Rosenblatt, M. (1952). Remarks on a multivariate transformation. *The Annals of Mathematical Statistics*, *23*(3), 470–472.

Vanem, E. (2015). Uncertainties in extreme value modelling of wave data in a climate change perspective. *Journal of Ocean Engineering and Marine Energy*, *1*(4), 339–359.

Velarde, J., Kramhøft, C., & Sørensen, J. D. (2018). Uncertainty Modeling and Fatigue Reliability Assessment of Concrete Gravity Based Foundation for Offshore Wind Turbines. In *The 28th International Ocean and Polar Engineering Conference*.

Winterstein, S. R., Ude, T. C., Cornell, C. A., Bjerager, P., & Haver, S. (1993). Environmental parameters for extreme response: Inverse FORM with omission factors. *Proceedings of the ICOSSAR-93, Innsbruck, Austria*, 551–557.